WAVE ROTOR GASDYNAMICS FOR AN AEROPROPULSION SYSTEM

Koji OKAMOTO
Department of Aeronautics and Astronautics,
School of Engineering, The University of Tokyo
7-3-1, Hongo, Bunkyo-ku, Tokyo, JAPAN

Keywords: *wave rotor, shock waves, unsteady flows*

Abstract

Wave rotors are expected to have a potential of improving drastically the performance of an aeropropulsion system. However, there are some problems in the operation at off-design conditions, because of its working principle that is not conventional. Furthermore, the gas dynamic states inside of the cells are very complicated even at the design point, because shock and rarefaction waves are reflected and interact with the contact discontinuity. It is therefore very important to investigate the inner flow of the wave rotor. One of the objectives in this study is to visualize this inner flow both experimentally and by numerical approach. In the experiments, optical image processing was utilized to support the instantaneous wall static pressure measurements, whilst, in the computations, an attempt was made to clarify the details of wave-coupled fluid motion based upon 2D Navier-Stokes equations. In addition, "gradual opening effects" on the inner flow are also investigated by changing the width of the cell.

The results of computations and experiments were in good agreement in terms of the intensity and the propagating velocity of the shock waves generated in the cells. As for the gradual opening effects, the greater influence was observed on the contact discontinuity than on the shock waves.

1 Introduction

The wave rotor is a kind of superchargers and its working principle is not conventional. The wave rotor consists of a rotor and ports as shown in Fig.1, and the rotor consists of many narrow channels called "cells", in which the working gas compression / expansion takes place. Each port charges or discharges the cells with fresh air or combustion gas, respectively.

Here, the working principle of the wave rotor is briefly addressed. Although there are several kinds of wave rotors, "4-port reverse flow type" [1] is adopted in this study. Fig.2 is called as the "wave diagram", which shows schematically the inner flow states of the wave rotor by spreading cylindrically arranged cells into a plane. At first (at the top of the rotor in Fig.2), the cell is filled with fresh air from the compressor.

[The Compression Process] When the cell is exposed to Gas-HP (High pressure Port), the hot gas from the burner (the pressure ratio is more than 2.0) rushes into the cell and "primary shock wave" is generated. This shock wave propagates to the left and reflects at the end wall. The reflected shock wave is called "secondary shock wave". By these two shock waves, the air is compressed and rushes into Air-HP that is opened to the cell just after the shock reflection. When the secondary shock wave reaches to the right end wall, Gas-HP is closed and a rarefaction wave is generated by the inertia of the gas. When this rarefaction wave reaches to the left end wall, Air-HP is closed.

[The Expansion Process] When the cell is exposed to Gas-LP (Low pressure Port), the gas in the cell flows out to the port, and a rarefaction wave is generated to propagate to the left end wall. When this wave reaches to the left end wall, Air-LP is opened to the cell and fresh air flows into the cell. When the cell is filled with the fresh air, these two ports are closed. By these processes, the condition in the cell becomes the same as that at the beginning of the cycle, so a cycle is completed.

By applying the wave rotor to a gas turbine, it will be possible to increase the peak cycle temperature and the total pressure ratio without increasing T5 (TIT) as shown in Fig.3 [2]. The wave rotor does not require a cooling system, because hot gas and fresh air flow into the cells alternately. Furthermore, the wave rotor is relatively light, because the compression is carried out not by mechanical but by shock waves.

In spite of these advantages, the wave rotor topped gas turbine has not yet been put into practical use, because there are some problems in operation at off-design conditions. Also, the inner flow states are very complicated even at the design point, because the shock and rarefaction waves are reflected and interact with the contact discontinuity.

There are very few experimental studies on the inner flow of wave rotors including visualization, due to the difficulty of measurement at high-speed rotor rotation. In addition, it is reported that the "gradual opening effects", meaning that the ports are gradually opened to the cells, have large influence on the performance of the wave rotor [3].

In the present study, a new approach will be shown to clarify the above points. The experimental and computational models are first introduced, then the results are compared each other, with a particular interest on the "gradual opening effects".

2 Computational Model

The unsteady, compressible 2-D Reynolds averaged Navier-Stokes equations with laminar viscosity are used as the governing equations in this study. The cells are cut at a mean rotor radius to be arranged into a 2-D reference plane. The solution scheme is based upon FDM (Finite Difference Method) discretization incorporating an implicit Chakravathy-Osher's 3rd order upwind TVD scheme with the van Leer's differentiable limitter. LU-ADI method with Newton iteration is also adopted for the time integration. The present numerical investigation is focused on the two shock waves, "primary" and "secondary", in the compression process.

The calculation conditions and meshes are listed in Table1, where "τ" is a parameter showing the gradual opening effects. In case of practical wave rotors, τ should be less than 1.0, because the compression wave at the beginning of the cycle must become a shock wave when it reaches to the other end of the cell. Three cases, including the one that τ is more than 1.0, are examined for comparison.

	Case 1	Case 2	Case 3
Length [m]	0.186	0.186	0.186
Width [m]	0.008	0.012	0.016
mesh	601 x 31	601 x 46	601 x 61
τ	0.555	0.832	1.109

$$\tau = \frac{passage\ opening\ \ time}{wave\ travel\ \ time} = \frac{b}{w}\cdot\frac{a}{L}$$

a: sound speed
b: cell width
L: cell length
w: rotor rotation speed
τ: the parameter of gradual opening effects

Table 1

The boundary conditions of the inflow and outflow need to be carefully treated since it is not to known whether the flow velocity at each point is supersonic or subsonic before the calculation is started. Therefore, locally one-dimensional Riemann problem was solved by applying the Riemann invariance at the boundaries to get the appropriate values. The values at each port are listed in Table 2, which were taken to be the outside values in adjacent

to the cell region. The gradual opening effects were simulated by gradually replacing the wall boundary condition by the corresponding inflow or outflow boundary conditions. To decide the timing of the opening and closing of the ports, the theoretical propagating velocity of a shock wave was used, which is also shown in Table 2. At the wall boundary, non-slip condition was assigned.

	Gas-HP	Air-HP
Total Pressure [atm]	2.55	1.0
Total Temperature [K]	288	288
Velocity [m/s] (axial direction)	140	0.0
Velocity [m/s] (circumferential direction)	26.4	0.0
Opening timing [degree] (0.0 means the beginning of the cycle)	0.0	30.0
Closing timing [degree]	10.0	35.0

Table 2

3 Experiments

3.1 Concept & Basic Design

To visualize the inner flow of a wave rotor, test equipment with a new concept was adopted in the experiments (Fig.4). The cells, supposed to be rotating, were fixed, whilst the ports, fixed originally, were in rotation. A care is therefore needed that the “rotors” in Fig.4 means the rotating ports to charge / discharge the working gas. Presently, only a single cell was installed in the test section that is made of acrylic resin, so that the reflecting schlieren method was able to be employed for visualization. The wall static pressure along the cell axis was also measured at the same time. Although compressed air was used for the combustion gas, it is called the “gas” hereafter for convenience.

The design particulars of this equipment are that the cell length is 186mm, its height is 16mm, and its width is 8mm or 16mm. These values were the same for Cases 1 and 3 in the Table 1. The rotor speed was 4200rpm and the mean radius of the ports (and the cell) is 60.0mm, yielding the rotation speed of 26.4m/s. These values were also given as the calculation conditions.

3.2 Working Gas Charge & Discharge

The gas coming from the compressor flows into the rotor of the gas side through the rotating shaft. After that, the gas flows into the cell, through Gas-HP, generates shock waves, and flows out to the atmosphere through Gas-LP. On the other hand, the air flows into the cell through Air-LP of the rotor at the air side, and is compressed by shock waves. After that, the air flows into Air-HP, and flows out to the atmosphere through the rotating shaft at the air side.

3.3 Visualization & Measurement

Fig.5 summarizes the whole experimental system.

Visualization was made by the reflecting schlieren method with a mercury-vapor lamp as the light source. A high-speed digital CCD camera was employed to take schlieren pictures.

To measure the wall static pressure, seven holes were arranged in the axial direction on each sidewall, wherein dynamic pressure transducers can be attached flush on the sidewall surface. Fig.5 also shows a detail of the measuring positions.

4 Results

4.1 Wall Static Pressure

4.1.1 Numerical and Experimental Comparison

Fig.6 shows the comparison of the measured and computed wall static pressure at each measuring position when the cell width is 8mm.

An excellent agreement is apparent between the computations and measurements. Although the difference at P1 and P8 is larger in magnitude than those at the other positions, this difference seems to be caused by the non-uniformity of the flow in Gas-HP and the clearance effects between the cell and the end wall. At P1, the computation shows a sudden decrease when the delay time is about 200μs, which is resulted from the “captured gas” (see

Figs.9, 10 and 11 in 3.2.1). On the other hand, the measured P1 doesn't show this sudden decrease. The disagreement may be caused by the difference of the inflow angle due to the clearance flow between the cell and the end wall.

4.1.2 Gradual Opening Effects

Fig.7 shows a comparison of the computed wall static pressure at P10 amongst Cases 1, 2 and 3 in Table 1. Intensity of the primary shock wave is inversely proportional to the cell width. Whilst, the cell width has little influence on the propagating speed of the primary and secondary shock waves.

Fig.8 shows a comparison of experimental measurements of the wall static pressure at P10 between the cases of the cell width 8mm and 16mm, which yields the same tendency as observed in the computation.

4.2 Flow Visualization

4.2.1 Computed Density Contours

The computed non-dimensional density contours of Cases 1, 2 and 3 are shown in Figs.9, 10 and 11, in which the "delay time (DT)" indicates the time elapsed from the instance of Gas-HP opening. The comparison indicates that the shape of the primary shock wave is not influenced by the gradual opening effects, although the thickness of those shock waves (or compression waves) is influenced. On the other hand, the contact surface is much influenced by the gradual opening effects. At the beginning of Gas-HP opening, the gas flows into the cell almost in the axial direction. After that, the inflow direction is turned in the direction opposite to the cell rotation (in the figures, the upper direction) by a vortex induced by the shear stress of the inflow. Due to the latter inflow, the region called "captured gas" is formed, wherein the gas state and the volume of this captured gas region are influenced by the gradual opening effects.

When the primary shock wave reaches to the end of the air side, the secondary shock wave is generated by reflection at the end wall. Here, it is noticed that Air-HP is partially opened to the cell at the moment when the reflection occurs, and the opened width of each case is the same. In other words, the wider the width of the cell, the larger the area of the wall part relative to the opening. Therefore, the intensity of the secondary shock wave is directly proportional to the cell width.

During the propagation of the secondary shock wave to the gas side, the shock wave interacts with the contact surface. The magnitude of this interaction is influenced by the strength of the generated vortex, hence, by the gradual opening effects.

4.2.2 Schlieren Pictures

Figs.12 and 13 show the schlieren pictures corresponding to the cases of cell width of 8mm and 16mm, respectively. In both cases, when the delay time is 500μs, the primary shock wave becomes visible for the first time. After the reflection (DT~530μs), the secondary shock wave is observed in both cases. A branched shock wave was appeared only in the Fig.13 when the delay time was 1100μs at the interaction of the shock wave and the contact surface. The similar phenomenon was also predicted in the results of computation (Fig.14). A slight difference in the shock wave positions between Figs.12 and 13 at each delay time was due to a small error of the delay time.

5 Conclusions

Unsteady wave rotor flow dynamics was analyzed both experimentally and by numerical approach. The results showed excellent agreement in view of the propagating speed and the intensity of the shock waves.

As for the gradual opening effects, both the experimental and numerical results showed the same tendency. That is, the gradual opening effects have a large influence on the intensity of the primary shock wave and the states of the contact discontinuity, whilst it has little influence on the propagating speed and the shape of the primary and secondary shock waves.

References

[1] Gyarmathy G. How Does the Comprex Pressure-Wave Supercharger Work? SAE Paper 830234, 1983.

[2] Welch G.E., Jones S.M., Paxson D.E. Wave Rotor-Enhanced Gas Turbine Engines. NASA Technical Memorandum 106998, 1995.

[3] Wilson J. An Experimental Determination of Losses in a 3-Port Wave Rotor. ASME Paper No. 96-GT-117, 1996.

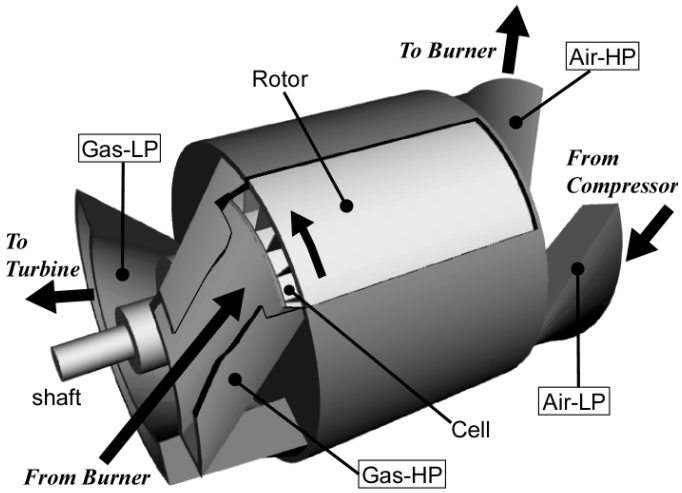

Fig.1 Wave Rotor

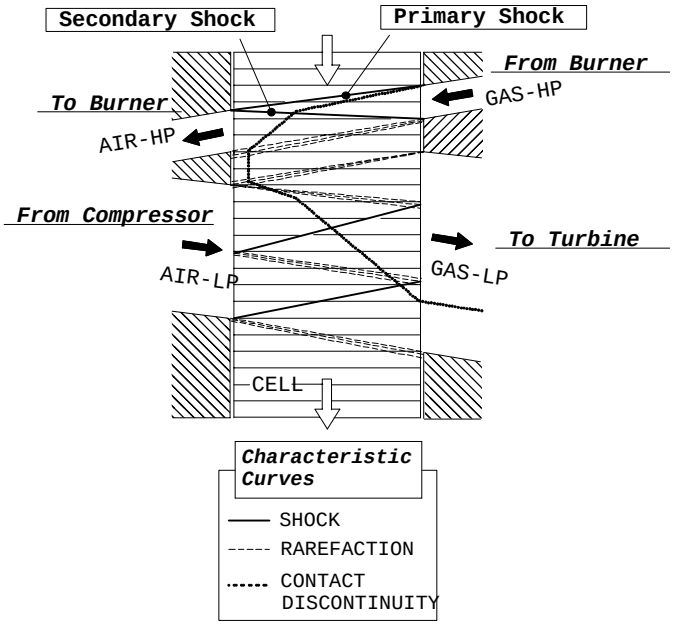

Fig.2 Wave Diagram

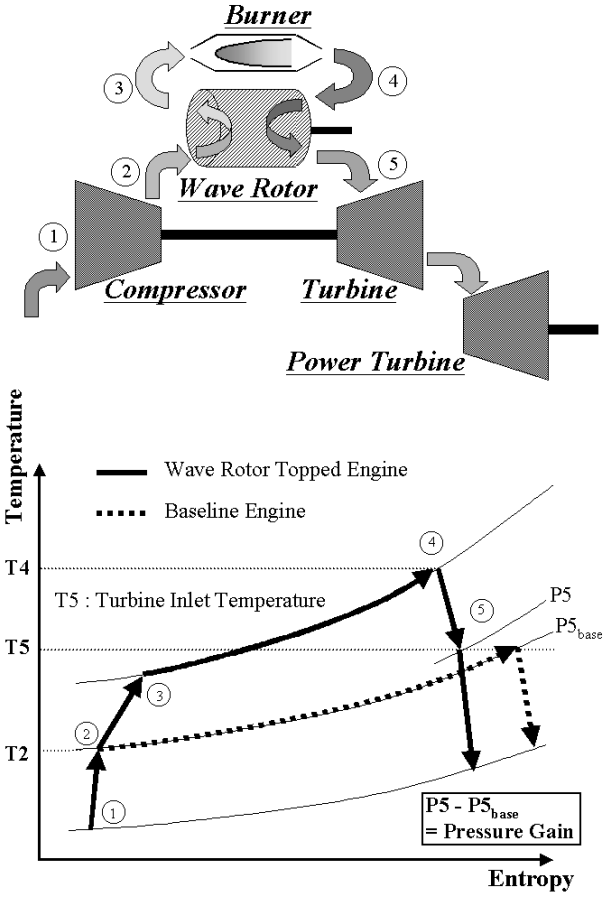

Fig.3 Topping Cycle

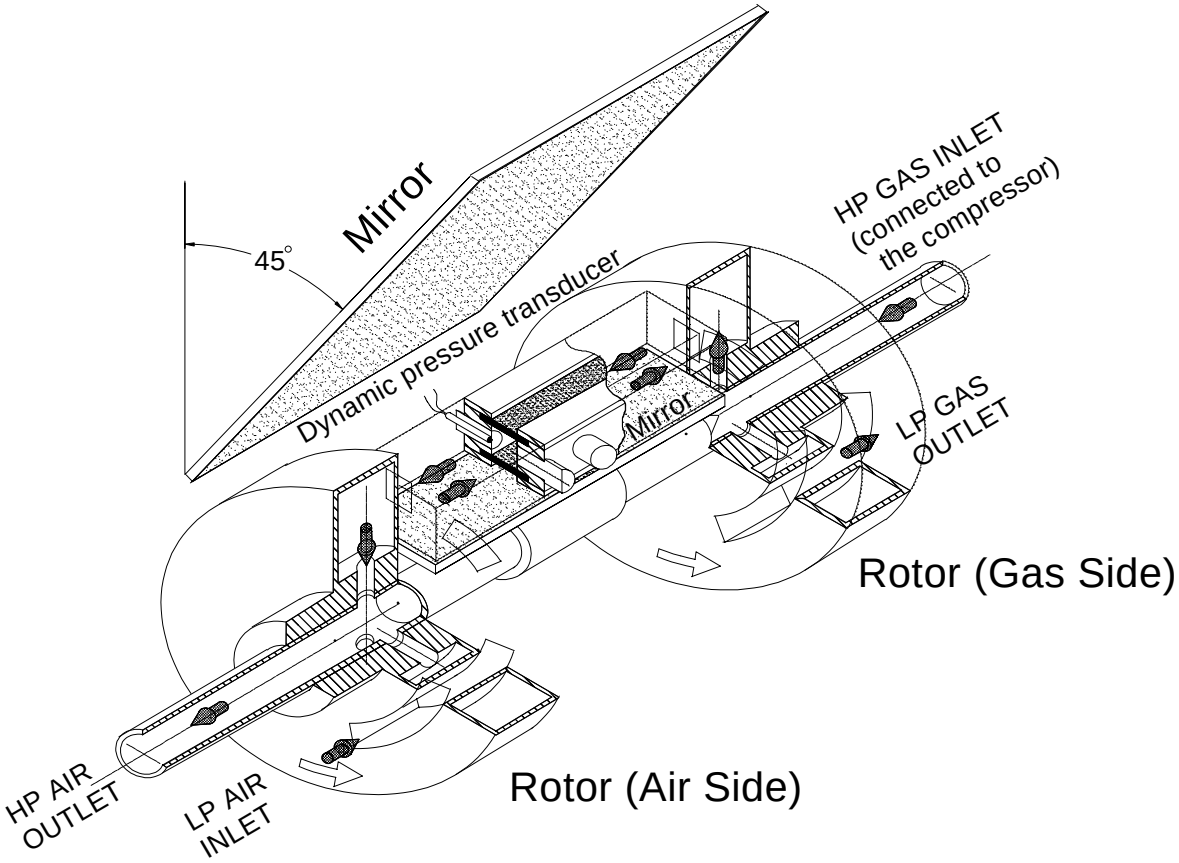

Fig.4 The Experimental Arrangements

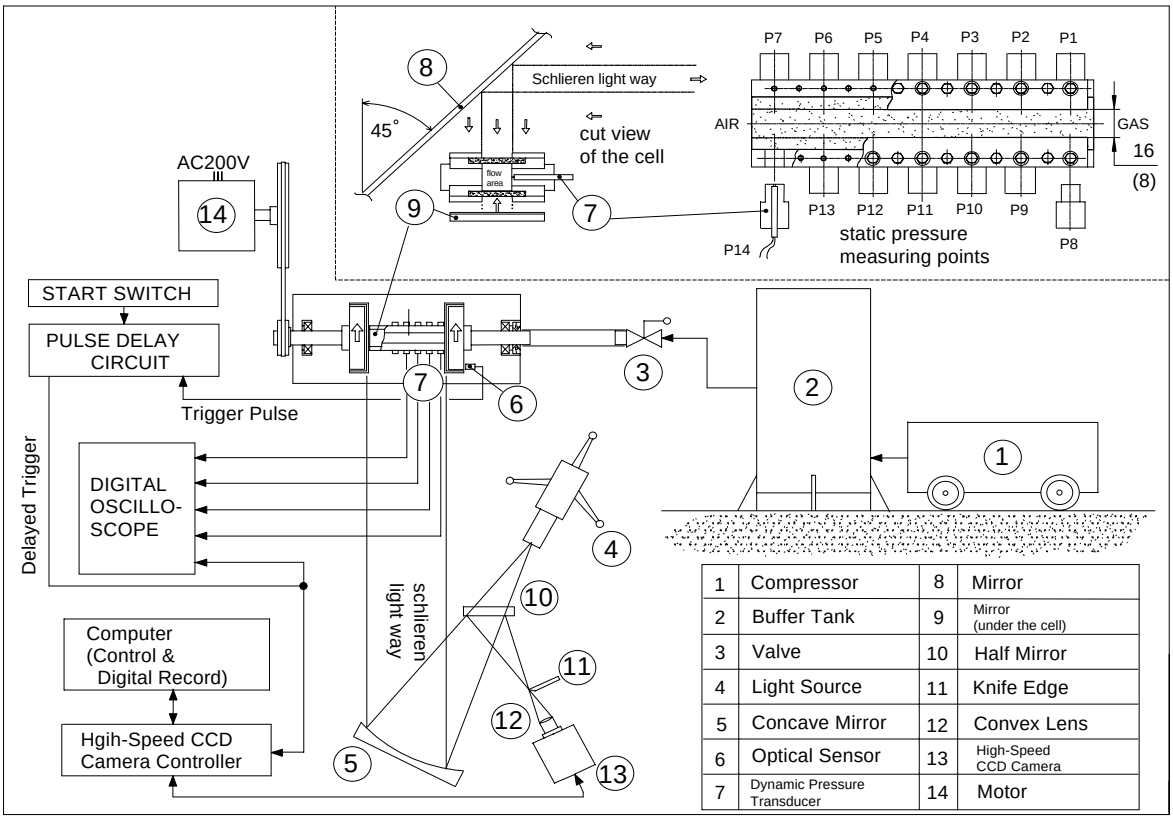

Fig.5 The Total Experimental System

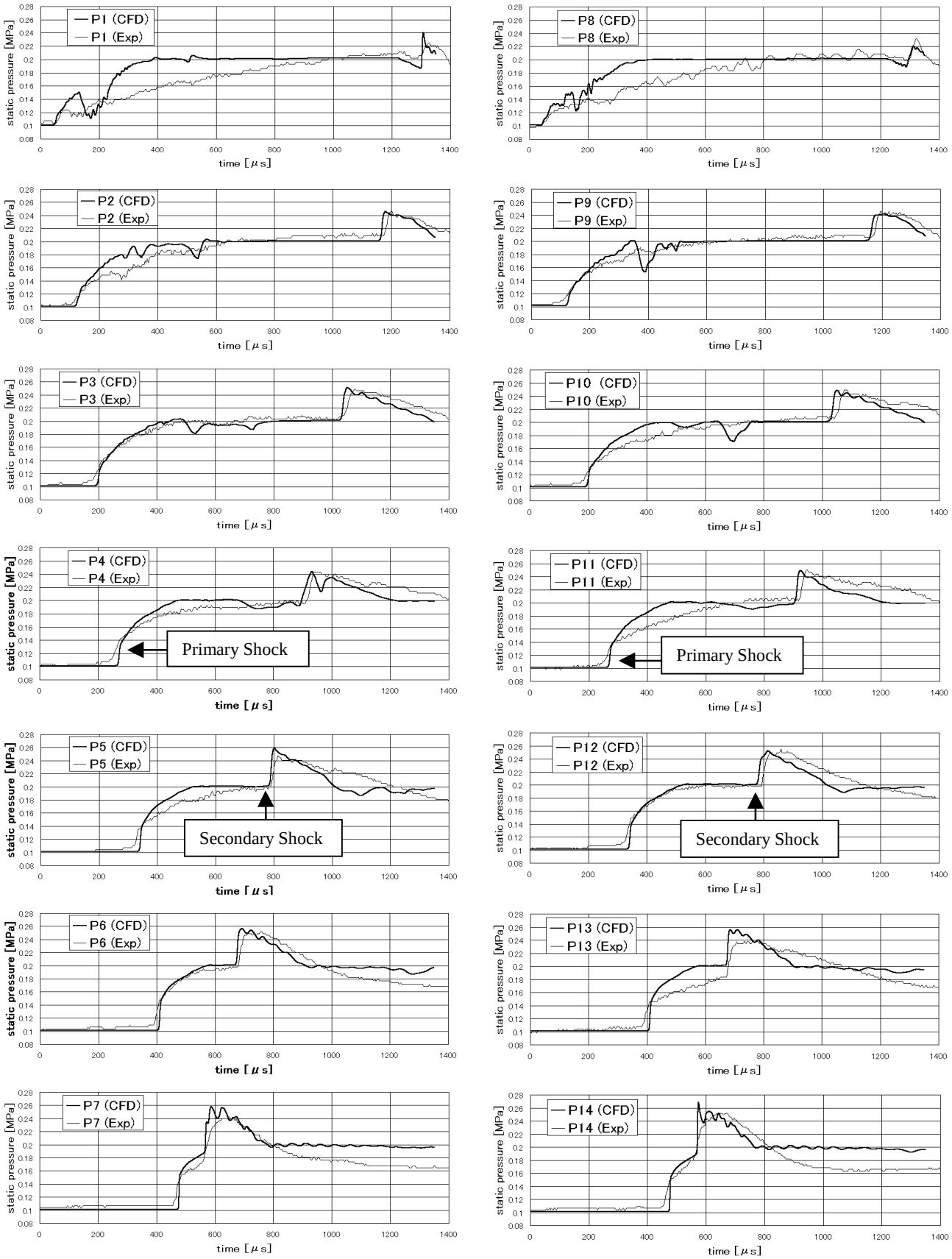

Fig.6 Comparison of Static Pressures at Various Axis Positions (Cell Width: 8mm)

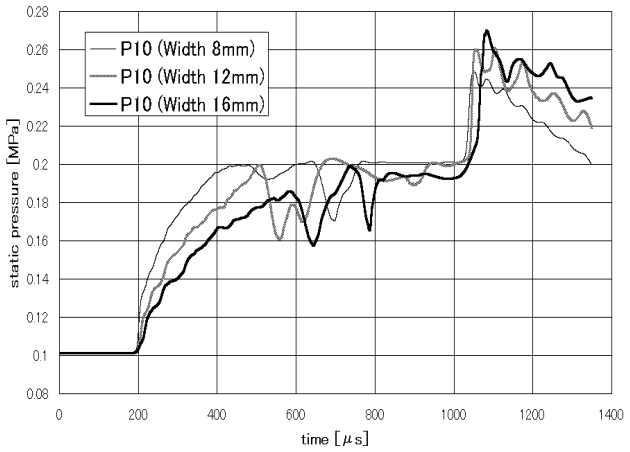

Fig.7 Comparison between Cases 1, 2 and 3 (P10 of CFD results)

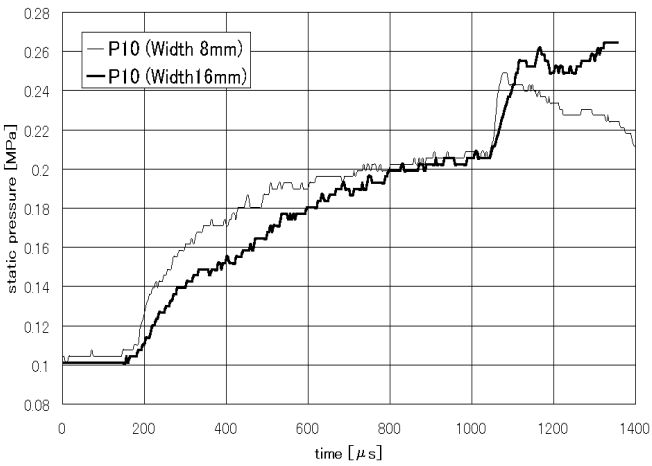

Fig.8 Comparison between Cases 1 and 3 (P10 of Experimental results)

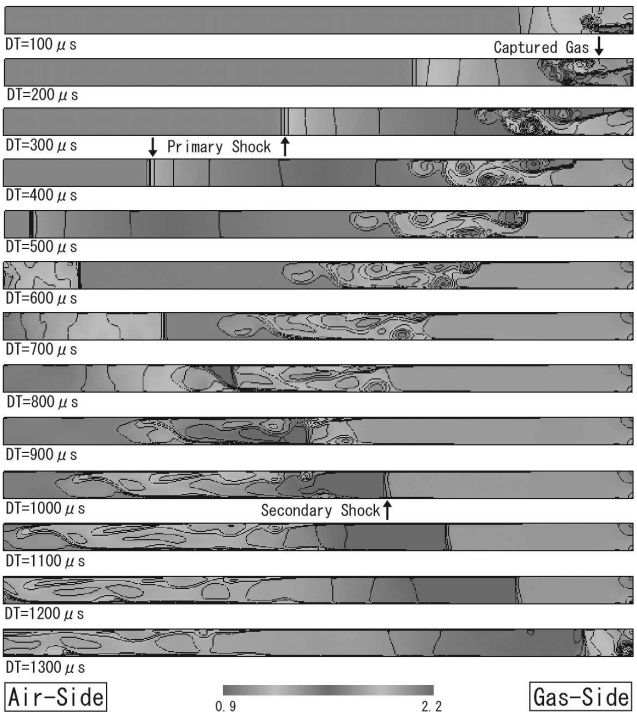

Fig.9 Non-Dimensional Density Contour (Case 1)

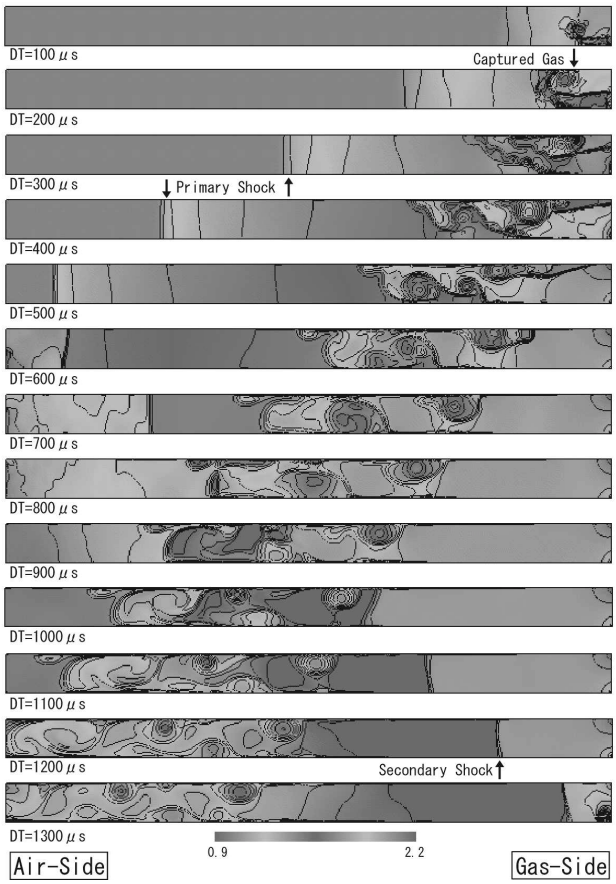

Fig.10 Non-Dimensional Density Contour (Case 2)

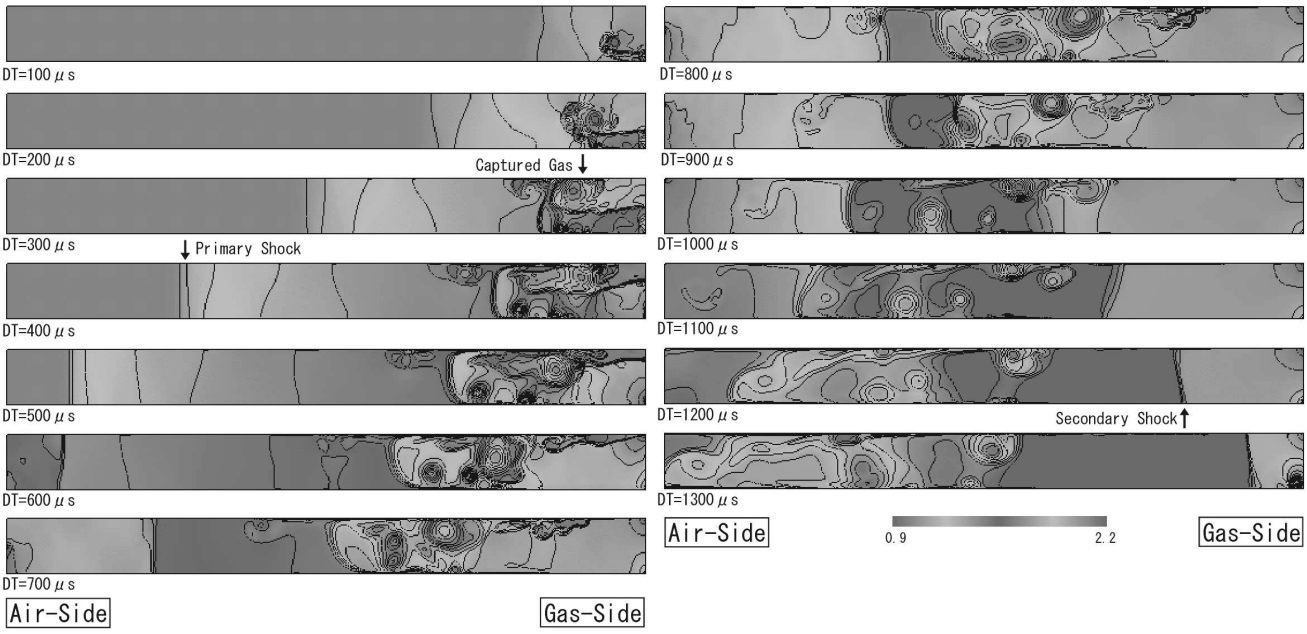

Fig.11 Non-Dimensional Density Contour (Case 3)

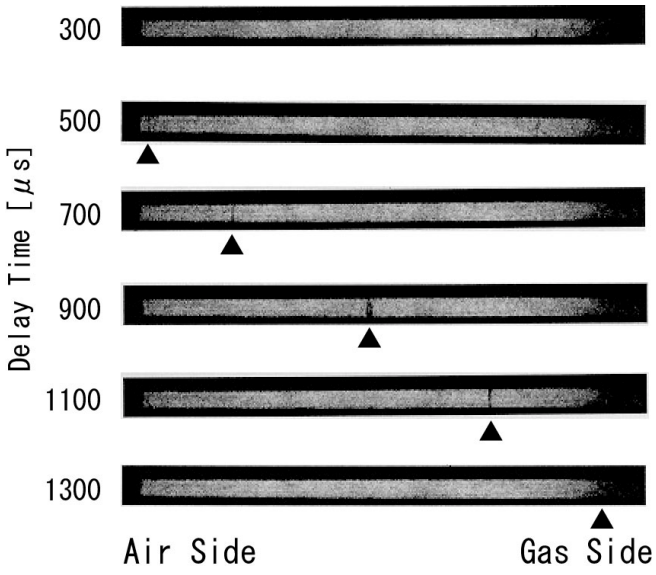

Fig.12 Schlieren Pictures (Width 8mm)

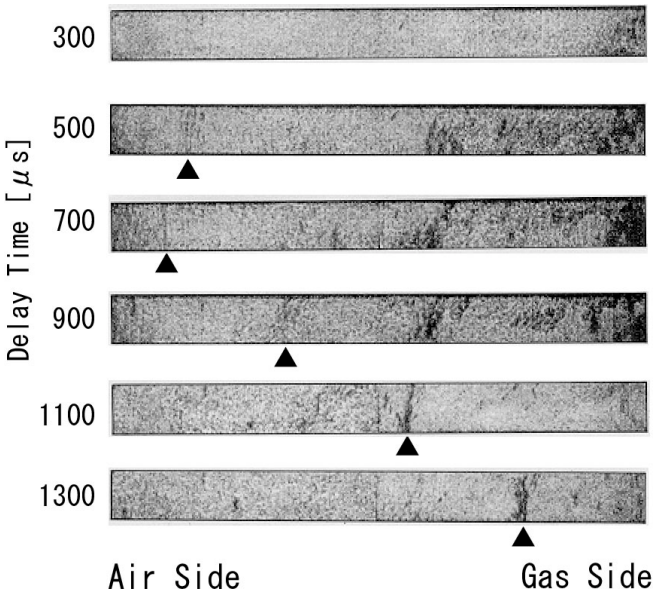

Fig.13 Schlieren Pictures (Width 16mm)

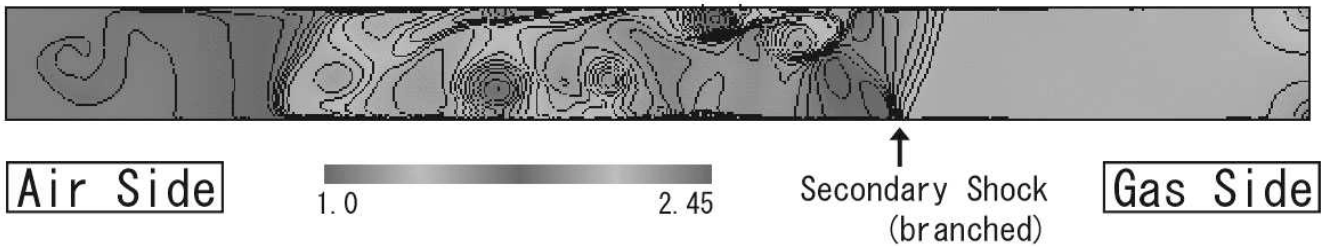

Fig.14 Appearance of Branched Secondary Shock Wave
(Non-dimensional Density Contour, CFD, Width: 16mm, DT=1100μs)